Technical Physics, 2022, Vol. 67, No. 2

15

Simulation of the ultracold neutron source at the reactor PIK

© *A.K. Fomin, A.P. Serebrov*

B.P. Konstantinov Petersburg Nuclear Physics Institute of National Research Center „Kurchatov Institute“,
188300 Gatchina, Leningrad Region, Russia
e-mail: fomin_ak@pnpi.nrcki.ru

Received September 21, 2021
Revised November 9, 2021
Accepted November 10, 2021

The paper presents the simulation of a complex of reserch with ultracold neutrons at the reactor PIK (Gatchina, Russia). The complex is being built on the basis of a high-intensity source of ultracold neutrons at the channel GEK-4. A Monte Carlo model has been developed, which includes a source, a neutron guide system and an experimental setup for search for the electric dipole moment of a neutron, taking into account their real location in the main hall of the reactor. Using the developed computer model the density of ultracold neutrons in the setup was obtained, which is $200\,\mathrm{cm}^{-3}$. It is 50 times higher than at the source at the Institut Laue-Langevin (Grenoble, France). This density will allow to achieve a sensitivity of measurements in the experiment of $1 \cdot 10^{-27}$ e· cm/year.

Keywords: ultracold neutrons, high intensity source, superfluid helium.

DOI: 10.21883/TP.2022.02.52959.261-21

Introduction

NRC „Kurchatov Institute“–PNPI is creating a complex for research with ultracold neutrons (UCN) using the PIK reactor [1]. The complex is based on a high-intensity UCN source where superfluid helium is used. Neutrons of very low energies ($\sim 10^{-7}$ eV), called ultracold, are unique because they can be stored in material and magnetic traps [2–4]. This provides wide methodical opportunities for precision experiments and study of fundamental physical issues. The condition for neutron reflection from a trap wall is $v_n < v_b$, where v_n is the velocity vector projection onto the normal to the surface, v_b is the boundary velocity of the wall material. Another important property of UCN is their exposure to the gravitational field of the Earth and movement along parabolic trajectories, the maximum lifting height being limited by their energy. The possibility of neutron storage in reservoirs was indicated by Ya.B. Zeldovich [5], and the first experiment for UCN extraction from a reactor was carried out in 1968 at Joint Institute for Nuclear Research (Dubna, Russia) [6]. UCN are being currently widely used for basic research: for search of the neutron electric dipole moment (EDM), for measurement of neutron lifetime, for measurement of neutron decay asymmetries etc. Accuracy of such experiments is limited by statistics, therefore it is vital to develop new high-intensity UCN sources [7].

The neutron EDM search experiment is related to the general problem of the theory of elementary particles: an adequate description of processes taking place with a violation of the CP- and T-symmetry. EDM value in contemporary theoretical models arises in the first order in the weak interaction and is approximately 10^{-26}–10^{-28} e · cm. The neutron EDM search was initiated in the 1950 [8]. The subsequent measurement history can be found in Particle Data Group [9]. The best experimental limitation on the neutron value at present is $|dn| < 1.8 \cdot 10^{-26}$ e · cm (90% C.L.) [10]. Measurements on the PIK reactor will be performed using a differential magnetic resonance spectrometer with two UCN storage chambers [11]. A Monte-Carlo-model of the experiment on the PIK reactor has been developed to obtain the absolute value of UCN density in the EDM spectrometer.

1. UCN sources based on superfluid helium

The main element of the source is a chamber filled with superfluid helium at the temperature of 1 K, which converts cold neutrons into UCN. The source is located on the beam of the GEK-4 channel. Ultracold neutrons originate in helium from cold neutrons having the wavelength of 9 Å. Neutrons, whose velocity exceeds the boundary velocity of the chamber wall coating, pass through the wall, while UCNs are accumulated up to a density determined by the time of storage in the chamber, and can be delivered via a neutron guide into an experimental setup. Storage time is determined by superfluid helium temperature and coefficient of losses at neutron collisions with the walls. Time of neutron storage in superfluid helium increases as temperature decreases, and is 100 s at the temperature of 1 K [12].

The results of calculations of achievable UCN density in a closed chamber are given below. The chamber has internal coating of ^{58}NiMo with the boundary velocity of 7.8 m/s and loss coefficient of $3 \cdot 10^{-4}$. When $\Phi(\lambda = 9\,\text{Å}) = 1 \cdot 10^9\,\mathrm{cm}^{-2}\mathrm{s}^{-1}\text{Å}^{-1}$, rate of UCN generation in superfluid helium is $100\,\mathrm{cm}^{-3}\mathrm{s}^{-1}$. The source chamber volume is 35 l. The diameter of the liquid helium supply pipeline is 1 cm. Heat gains from superfluid helium are

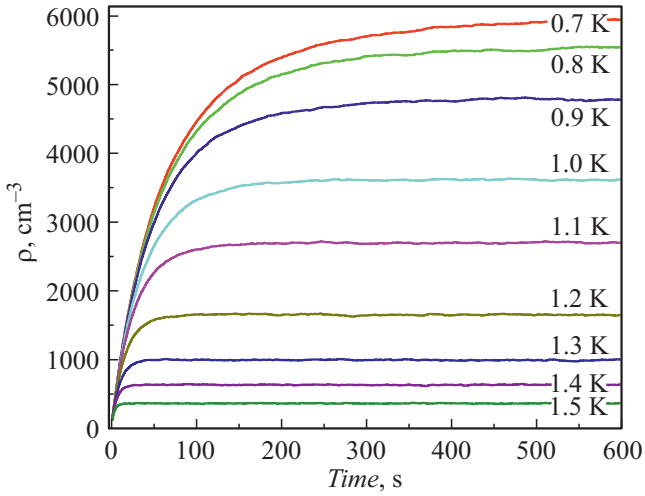

Figure 1. Trend of UCN accumulation in a closed chamber of a source at different superfluid helium temperatures. The loss coefficient for chamber wall coating is equal to $3 \cdot 10^{-4}$.

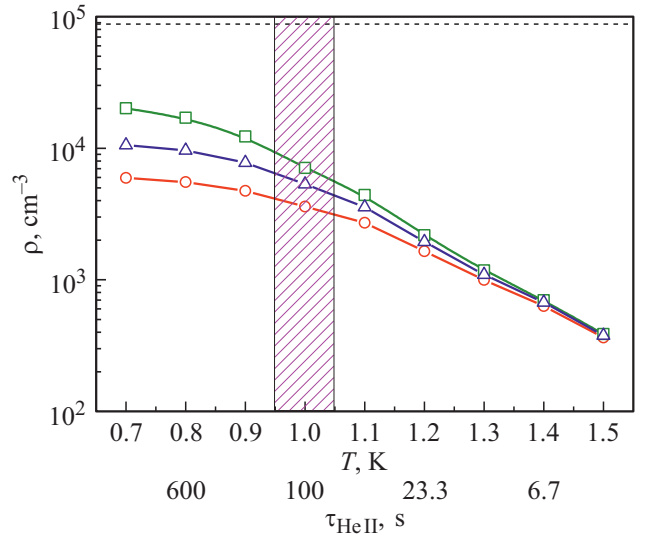

Figure 2. UCN density in the closed chamber of the source depending on superfluid helium temperature in the source chamber. Loss coefficient for chamber wall deposition: squares — 0, triangles — $1 \cdot 10^{-4}$, circles — $3 \cdot 10^{-4}$. The dashed line shows the UCN density achievable in case of no losses upon collisions with the walls and in superfluid helium.

withdrawn via a heat exchanger. The trend of UCN accumulation in the source chamber at different temperatures is shown in Fig. 1. The statistical uncertainties in the calculations are less than 0.5% and so are omitted from the figures. The UCN density in the steady-state condition depending on temperature for different loss coefficients is shown in Fig. 2. The UCN density in the closed chamber of the source at the temperature of 1 K and the loss coefficient for chamber wall deposition of $3 \cdot 10^{-4}$ is $3.5 \cdot 10^3$ cm^{-3}.

2. Test bench

Manufacture of a UCN source requires the appropriate quality of its components. UCN density in the experiment will be the higher, the better the neutron storage in the source chamber and the better the pass-through capacity of the neutron guide system. Testing of the source structural elements is performed using a dedicated test bench (Fig. 3), which can be used on the existing UCN sources. The bench can be used for testing of UCN storage in the source chamber (Fig. 3, *a*), or for testing of passage through the neutron guide system from the source to the experimental setup (Fig. 3, *b*). Thereat, a neutron guide system can comprise such elements as turns, branching tees, membrane units etc. A Monte-–Carlo model of the bench has been developed for calculations in different bench operation modes.

Turbulator *1* for cut-off of abovebarrier neutrons in the spectrum [13] is installed at the bench inlet. The turbulator is a chamber where two neutron guides are inserted from different sides so as to prevent direct transit of neutrons from one neutron guide to the other one. Thus, neutrons passing through it make several collisions, and abovebarrier neutrons are most probably screened out. The turbulator is made of stainless steel with the boundary velocity of 6.2 m/s and loss coefficient of $3 \cdot 10^{-4}$. The Maxwell spectrum was enacted at the turbulator inlet. After the turbulator, neutrons enter the neutron guide with a gate *2*. The neutron guide diameter is 138 mm, the gate diameter is 137 mm. After the neutron guide, neutrons enter storage chamber № 1 *3*. The chamber and the neutron guide are deposited with NiMo having the boundary speed of 6.55 m/s and loss coefficient of $3 \cdot 10^{-4}$ [14]. A neutron guide, going to the UCN detector of storage chamber № 1 *4*, is connected to the chamber bottom. The diameter of the chamber outlet hole is 11 mm. Then either a plugged adapter (Fig. 3, *a*) or

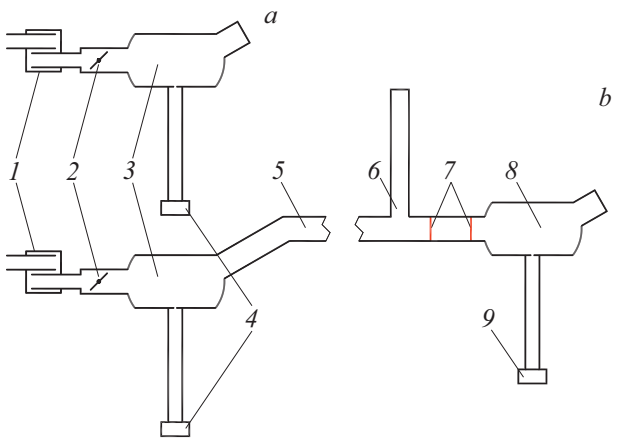

Figure 3. Layouts of the assembled test bench: *a* — for testing of UCN storage in the chamber, *b* — for testing of UCN passage through the neutron guide system. *1* — turbulator, *2* — gate, *3* — storage chamber № 1, *4* — UCN detector of storage chamber № 1, *5* — neutron guide, *6* — tee, *7* — Al-membranes, *8* — storage chamber № 2, *9* — UCN detector of storage chamber № 2.

a neutron guide *5* with the diameter of 138 mm (Fig. 3, *b*) is connected to the chamber. The neutron guide is equipped with a tee *6* and two Al membranes *7*. Storage chamber № 2 *8* with UCN detector *9* is connected to the other neutron guide end; their design is identical to chamber *3* with detector *4*. UCN reflections from the neutron guide walls are chiefly mirror ones, diffuse reflection probability is 0.7%. Diffuse reflection probability is 90% in case of UCN reflection from the chamber walls.

2.1. Modelling of neutron storage in a source chamber

The design of connection of the bench elements in case of modelling of neutron storage in a source chamber corresponds to Fig. 3, *a*. The corresponding count of UCN detector *4* is shown in Fig. 4. Neutrons start coming from the neutron source in the constant mode at time moment $t = 0$ s. In this case, the detector count is small since neutrons enter chamber *3* through the gap in gate *2*. The gate is open in a time interval of 200 to 300 s. When the gate opens, the count of detector *4* increases. The calculation was performed for several loss coefficients for the source chamber coating. Thus, a conclusion concerning the coating quality can be made based on the detector count pattern.

2.2. Modelling of passage through the neutron guide system

The design of connection of the bench elements in case of modelling of passage through the neutron guide system corresponds to Fig. 3, *b*. Neutron guide *5* exits chamber *3* at the angle of30°, and then turns to a horizontal position. This design was made in the UCN source to maintain the YXH superfluid helium level in the chamber. The total neutron guide length is 3.5 m. Tee *6* and two Al-membranes *7* are installed before chamber № 2. Inclusion of a tee into the system is due to the fact that one of the

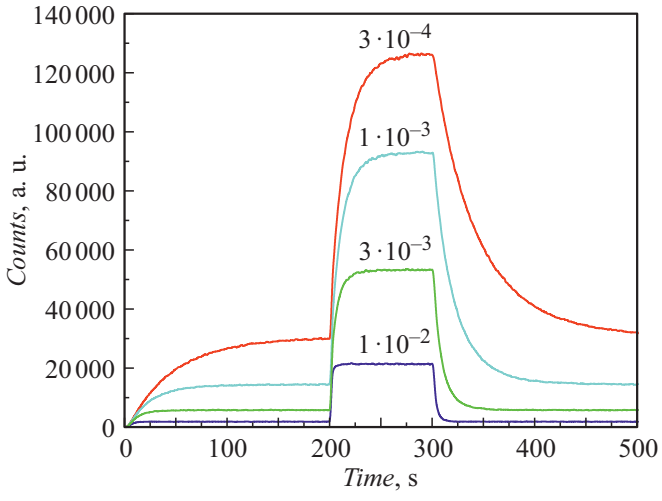

Figure 4. Detector count in case of chamber storage modelling for different wall coating loss coefficients.

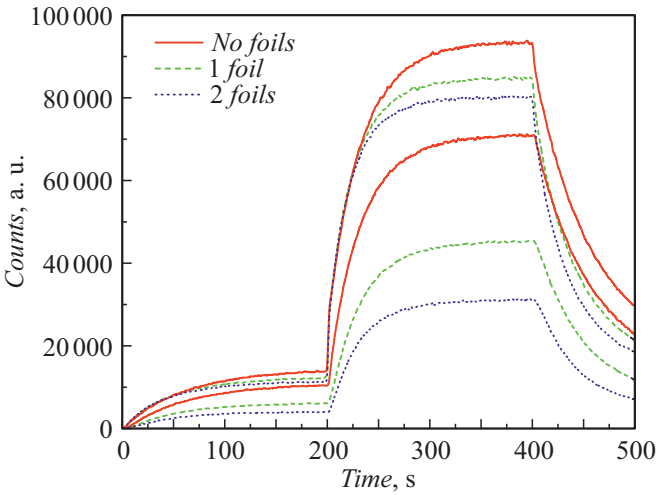

Figure 5. Time diagram of detector counts for neutron guide system variants: without membranes, with one membrane and with two membranes. The three upper curves correspond to the detector count of chamber № 1, the three lower ones — to the detector count of chamber № 2.

possible source designs is a variant where superfluid helium is cooled by pumping of its vapors through a pipeline. The pumping pipeline in this case approaches the neutron guide vertically and at the same time acts as a gravitational gate for UCN. The Al-membranes are intended for separation of volumes by vacuum. Since several experimental setups will be installed on the source, UCNs will be redirected from the source neutron guide to the setups via the beam splitter. The first membrane pertains respectively to the UCN source, and the second one — to the experimental setup. The membrane thickness is 100 μm, the boundary velocity is 3.2 m/s. The loss coefficient for coating of the storage chamber walls in this calculation is $3 \cdot 10^{-4}$. The corresponding counts of UCN detectors *4* and *9* are shown in Fig. 5 for different membrane quantities. The shutter is open in a time interval of 200 to 400 s. Pass-through capacity of the neutron guide system with various elements is estimated based on the difference of the counts of UCN detectors *4* and *9*. Thus, pass-through capacity for the given configuration is $\sim$ 75% without membranes, $\sim$ 53% — with one membrane, $\sim$ 38% — with two membranes.

3. UCN density in the EDM spectrometer

Search for the neutron EDM will be performed using a differential magnetic resonance spectrometer with two UCN storage chambers, a reversible electric field, a system of double polarization analysis and four detectors [11]. Statistical accuracy of measurements in the experiment is determined by the formula $\delta d_n = \frac{h}{4\pi\alpha E T\sqrt{N}}$, where α — quality parameter of the resonance curve, E — electric field intensity, T — time of neutron storage in resonance conditions, N — total neutron count within the experiment

time. Sensitivity estimation of the experiment on the PIK reactor requires a calculated value of UCN density in the setup.

The design model of the experiment on the PIK reactor is shown in Fig. 6, *a*. A straight neutron guide 140 mm in diameter goes from the source, and then it changes into two neutron guides with the cross-section of 25×85 mm which go to the EDM spectrometer chambers. The distance from the source chamber to the setup chambers is about 13 m. The neutron guides are inserted into and brought out of the spectrometer via the central electrode. The source chamber and neutron guides have internal coating of ^{58}NiMo with the boundary speed of 7.8 m/s and loss coefficient of $3 \cdot 10^{-4}$. The spectrometer traps have the radius of 263 mm and the height of 76 mm. The boundary velocity of the beryllium coating is 6.8 m/s, the loss coefficient is

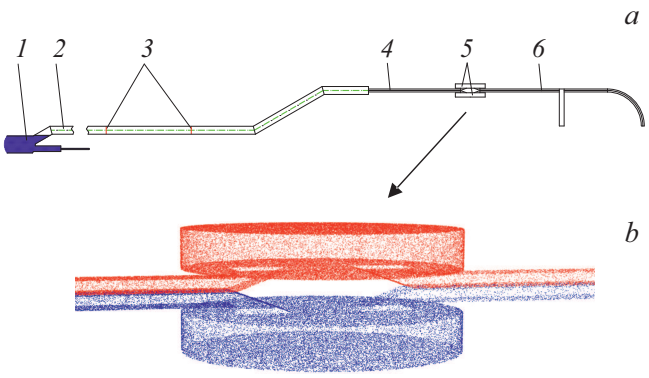

Figure 6. *a* — design model of the experiment for neutron EDM search using the PIK reactor: *1* — chamber of UCN source with superfluid helium, *2* — neutron guide 140 mm in diameter, *3* — two Al-foils, *4* — two neutron guides with the cross-section of 25 × 85 mm, *5* — EDM spectrometer chambers, *6* — neutron guides to four detectors. *b* — points of neutron collisions with the walls of the EDM spectrometer chambers obtained by means of a Monte-–Carlo model.

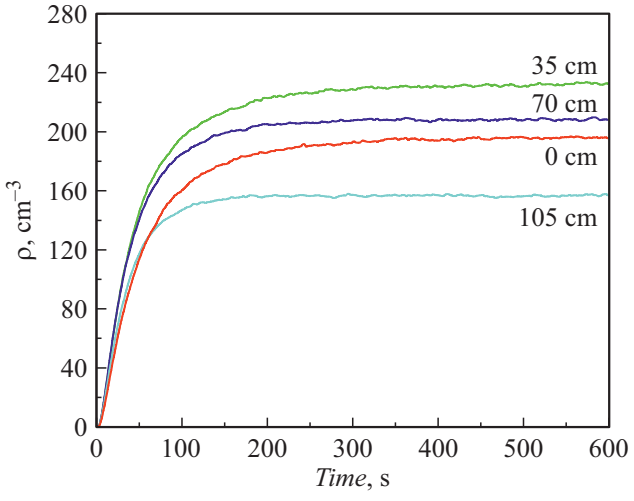

Figure 7. Time diagram of UCN density in the EDM spectrometer at different setup lifting heights.

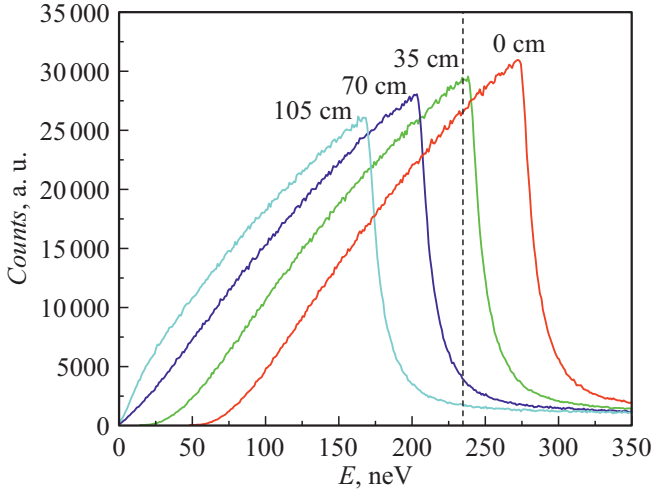

Figure 8. Spectra of neutrons in the neutron guide before the EDM spectrometer at different setup lifting heights. The dashed line shows the boundary energy of the spectrometer chamber coating equal to 235 neV.

$1.2 \cdot 10^{-4}$. A Monte-–Carlo model of the experiment has been developed where the history of each neutron is enacted from origination in the source till entry in the experimental volume, taking into account all possible losses. To illustrate operation of the Monte–Carlo model, Fig. 6, *b* shows the calculated points of neutron collisions with the walls of the EDM spectrometer chambers.

Variants with a lifted EDM spectrometer (installation on a platform) have been considered for restoration of the spectrum part which is cut off flow below by the Al-foil. This provides a softer UCN spectrum having a better storage time. In case of lifting, the neutron guide turning angle is 30°. The variants with lifting by 35, 70, 105 cm have been calculated. Fig. 7 shows the time diagram of UCN density in the EDM spectrometer. When lifted higher than 35 cm, the effect of spectrum cut-off from above appears in the UCN source chamber, resulting in a decreased UCN density in the EDM spectrometer. The corresponding neutron spectra are shown in Fig. 8. The modelling result is that the experiment on the PIK reactor can provide the density value of $\sim 200\,\mathrm{cm}^{-3}$.

Conclusion

The developed computer model has yielded a value of UCN density in the EDM spectrometer equal to $200\,\mathrm{cm}^{-3}$. The EDM spectrometer on the reactor at Institut Laue–Langevin (ILL) (Grenoble, France) has yielded the sensitivity of $\delta d_n \sim 1.7 \cdot 10^{-25}\,\mathrm{e \cdot cm/day}$, UCN density at the spectrometer inlet being $4\,\mathrm{cm}^{-3}$. When electric field intensity increases from 12–14 to 27 kV/cm [15], experiment sensitivity improves to $\delta d_n \sim 1 \cdot 10^{-25}\,\mathrm{e \cdot cm/day}$ on the ILL reactor. When UCN density in the spectrometer chambers is $200\,\mathrm{cm}^{-3}$, the sensitivity of

$\delta d_n \sim 1 \cdot 10^{-27}\,\mathrm{e}\cdot\mathrm{cm/year}$ can be obtained on the PIK reactor. Detection of the neutron EDM or a new limitation on its magnitude at such a level can become a decisive factor in the selection of a theory to adequately describe violations of the CP-symmetry.

Funding

The work has been performed within the framework of creation of the PIK reactor instrumental base.

Conflict of interest

The authors declare that they have no conflict of interest.

References

[1] M.V. Kovalchuk, V.V. Voronin, S.V. Grigoriev, A.P. Serebrov. Crystallogr. Rep., **66** (2), 195 (2021). DOI: 10.1134/S1063774521020061

[2] V. Ignatovich. *The Physics of Ultracold Neutrons* (Clarendon, Oxford, 1990)

[3] R. Golub, D. Richardson, S. Lamoreaux. *Ultra-Cold Neutrons* (Adam Hilger, Bristol, Philadelphia, NY., 1991)

[4] A. Steyerl. *Ultracold Neutrons* (World Scientific Publishing Company, Singapore, 2020)

[5] Ya.B. Zeldovich. ZhETF, **36**, 1952 (1959) (in Russian).

[6] V.I. Luschikov, Yu.N. Pokotilovsky, A.V. Strelkov, F.L. Shapiro. Pisma v ZhETF, **9**, 40 (1969) (in Russian).

[7] G. Bison, M. Daum, K. Kirch, B. Lauss, D. Ries, P. Schmidt-Wellenburg, G. Zsigmond, T. Brenner, P. Geltenbort, T. Jenke, O. Zimmer, M. Beck, W. Heil, J. Kahlenberg, J. Karch, K. Ross, K. Eberhardt, C. Geppert, S. Karpuk, T. Reich, C. Siemensen, Y. Sobolev, N. Trautmann. Phys. Rev. C, **95**, 045503 (2017). DOI: 10.1103/PhysRevC.95.045503

[8] J.H. Smith, E.M. Purcell, N.F. Ramsey. Phys. Rev., **108**, 120 (1957). DOI: 10.1103/PhysRev.108.120

[9] P.A. Zyla, R.M. Barnett, J. Beringer, O. Dahl, D.A. Dwyer, D.E. Groom, C.-J. Lin, K.S. Lugovsky, E. Pianori, D.J. Robinson, C.G. Wohl, W.-M. Yao, K. Agashe, G. Aielli, B.C. Allanach, C. Amsler, M. Antonelli, E.C. Aschenauer, D.M. Asner, H. Baer, Sw. Banerjee, L. Baudis, C.W. Bauer, J.J. Beatty, V.I. Belousov, S. Bethke, A. Bettini, O. Biebel, K.M. Black, E. Blucher, O. Buchmuller, V. Burkert, M.A. Bychkov, R.N. Cahn, M. Carena, A. Ceccucci, A. Cerri, D. Chakraborty, R. Sekhar Chivukula, G. Cowan, G. D'Ambrosio, T. Damour, D. de Florian, A. de Gouvêa, T. DeGrand, P. de Jong, G. Dissertori, B.A. Dobrescu, M. D'Onofrio, M. Doser, M. Drees, H.K. Dreiner, P. Eerola, U. Egede, S. Eidelman, J. Ellis, J. Erler, V.V. Ezhela, W. Fetscher, B.D. Fields, B. Foster, A. Freitas, H. Gallagher, L. Garren, H.-J. Gerber, G. Gerbier, T. Gershon, Y. Gershtein, T. Gherghetta, A.A. Godizov, M.C. Gonzalez-Garcia, M. Goodman, C. Grab, A.V. Gritsan, C. Grojean, M. Grünewald, A. Gurtu, T. Gutsche, H.E. Haber, C. Hanhart, S. Hashimoto, Y. Hayato, A. Hebecker, S. Heinemeyer, B. Heltsley, J.J. Hernández-Rey, K. Hikasa, J. Hisano, A. Höcker, J. Holder, A. Holtkamp, J. Huston, T. Hyodo, K.F. Johnson, M. Kado, M. Karliner, U.F. Katz, M. Kenzie, V.A. Khoze, S.R. Klein, E. Klempt, R.V. Kowalewski, F. Krauss, M. Kreps, B. Krusche, Y. Kwon, O. Lahav, J. Laiho, L.P. Lellouch, J. Lesgourgues, A.R. Liddle, Z. Ligeti, C. Lippmann, T.M. Liss, L. Littenberg, C. Lourengo, S.B. Lugovsky, A. Lusiani, Y. Makida, F. Maltoni, T. Mannel, A.V. Manohar, W.J. Marciano, A. Masoni, J. Matthews, U.-G. Meißner, M. Mikhasenko, D.J. Miller, D. Milstead, R.E. Mitchell, K. Mönig, P. Molaro, F. Moortgat, M. Moskovic, K. Nakamura, M. Narain, P. Nason, S. Navas, M. Neubert, P. Nevski, Y. Nir, K.A. Olive, C. Patrignani, J.A. Peacock, S.T. Petcov, V.A. Petrov, A. Pich, A. Piepke, P.A. Zyla, R.M. Barnett, J. Beringer, O. Dahl, D.A. Dwyer, D.E. Groom, C.-J. Lin, K.S. Lugovsky, E. Pianor A. Pomarol, S. Profumo, A. Quadt, K. Rabbertz, J. Rademacker, G. Raffelt, H. Ramani, M. Ramsey-Musolf, B.N. Ratcliff, P. Richardson, A. Ringwald, S. Roesler, S. Rolli, A. Romaniouk, L.J. Rosenberg, J.L. Rosner, G. Rybka, M. Ryskin, R.A. Ryutin, Y. Sakai, G.P. Salam, S. Sarkar, F. Sauli, O. Schneider, K. Scholberg, A.J. Schwartz, J. Schwiening, D. Scott, V. Sharma, S.R. Sharpe, T. Shutt, M. Silari, T. Sjöstrand, P. Skands, T. Skwarnicki, G.F. Smoot, A. Soffer, M.S. Sozzi, S. Spanier, C. Spiering, A. Stahl, S.L. Stone, Y. Sumino, T. Sumiyoshi, M.J. Syphers, F. Takahashi, M. Tanabashi, J. Tanaka, M. Taševský, K. Terashi, J. Terning, U. Thoma, R.S. Thorne, L. Tiator, M. Titov, N.P. Tkachenko, D.R. Tovey, K. Trabelsi, P. Urquijo, G. Valencia, R. Van de Water, N. Varelas, G. Venanzoni, L. Verde, M.G. Vincter, P. Vogel, W. Vogelsang, A. Vogt, V. Vorobyev, S.P. Wakely, W. Walkowiak, C.W. Walter, D. Wands, M.O. Wascko, D.H. Weinberg, E.J. Weinberg, M. White, L.R. Wiencke, S. Willocq, C.L. Woody, R.L. Workman, M. Yokoyama, R. Yoshida, G. Zanderighi, G.P. Zeller, O.V. Zenin, R.-Y. Zhu, S.-L. Zhu, F. Zimmermann, J. Anderson, T. Basaglia, V.S. Lugovsky, P. Schaffner, W. Zheng. Prog. Theor. Exp. Phys., **2020**, 083C01 (2020−2021). DOI: 10.1093/ptep/ptaa104

[10] C. Abel, S. Afach, N.J. Ayres, C.A. Baker, G. Ban, G. Bison, K. Bodek, V. Bondar, M. Burghoff, E. Chanel, Z. Chowdhuri, P.-J. Chiu, B. Clement, C.B. Crawford, M. Daum, S. Emmenegger, L. Ferraris-Bouchez, M. Fertl, P. Flaux, B. Franke, A. Fratangelo, P. Geltenbort, K. Green, W.C. Griffith, M. van der Grinten, Z.D. Grujić, P.G. Harris, L. Hayen, W. Heil, R. Henneck, V. Hélaine, N. Hild, Z. Hodge, M. Horras, P. Iaydjiev, S.N. Ivanov, M. Kasprzak, Y. Kermaidic, K. Kirch, A. Knecht, P. Knowles, H.-C. Koch, P.A. Koss, S. Komposch, A. Kozela, A. Kraft, J. Krempel, M. Kuźniak, B. Lauss, T. Lefort, Y. Lemiére, A. Leredde, P. Mohanmurthy, A. Mtchedlishvili, M. Musgrave, O. Naviliat-Cuncic, D. Pais, F.M. Piegsa, E. Pierre, G. Pignol, C. Plonka-Spehr, P.N. Prashanth, G. Quéméner, M. Rawlik, D. Rebreyend, I. Rienäcker, D. Ries, S. Roccia, G. Rogel, D. Rozpedzik, A. Schnabel, P. Schmidt-Wellenburg, N. Severijns, D. Shiers,. Tavakoli Dinani, J.A. Thorne, R. Virot, J. Voigt, A. Weis, E. Wursten, G. Wyszynski, J. Zejma, J. Zenner, G. Zsigmond. Phys. Rev. Lett., **124**, 081803 (2020). DOI: 10.1103/PhysRevLett.124.081803

[11] A.P. Serebrov, E.A. Kolomenskiy, A.N. Pirozhkov, I.A. Krasnoschekova, A.V. Vassiljev, A.O. Polyushkin, M.S. Lasakov, A.N. Murashkin, V.A. Solovey, A.K. Fomin, I.V. Shoka, O.M. Zherebtsov, P. Geltenbort, S.N. Ivanov, O. Zimmer, E.B. Alexandrov, S.P. Dmitriev, N.A. Dovator. Phys. Rev. C, **92**, 055501 (2015). DOI: 10.1103/PhysRevC.92.055501

[12] R. Golub, C. Jewell, P. Ageron, W. Mampe, B. Heckel, I. Kilvington. Z. Phys. B Con. Mat., **51**, 187 (1983). DOI:10.1007/BF01307673

[13] M. Daum, A. Frei, P. Geltenbort, E. Gutsmiedl, P. Höbel, H.-C. Koch, A. Kraft, T. Lauer, A.R. Müller, S. Paul, G. Zsigmond. Nucl. Instrum. Meth. A, **675**, 103 (2012). DOI: 10.1016/j.nima.2012.02.007

[14] V. Bondar, S. Chesnevskaya, M. Daum, B. Franke, P. Geltenbort, L. Göltl, E. Gutsmiedl, J. Karch, M. Kasprzak, G. Kessler, K. Kirch, H.-C. Koch, A. Kraft, T. Lauer, B. Lauss, E. Pierre, G. Pignol, D. Reggiani, P. Schmidt-Wellenburg, Yu. Sobolev, T. Zechlau, G. Zsigmond. Phys. Rev. C, **96**, 035205 (2017). DOI: 10.1103/PhysRevC.96.035205

[15] M.S. Lasakov, A.N. Pirozhkov, A.P. Serebrov. ZhTF, **89** (3), 475 (2019) (in Russian) DOI: 10.21883/TP.2022.02.52959.261-21 [M.S. Lasakov, A.N. Pirozhkov, A.P. Serebrov. Tech. Phys., **64** (3), 436 (2019). DOI: 10.1134/S1063784219030162]